

# A study of the relation between intensity oscillations and magnetic field parameters in a sunspot: Hinode observations

A. Raja Bayanna<sup>1</sup>, Shibu K Mathew<sup>1</sup>, Brajesh Kumar<sup>1</sup>, Rohan E. Louis<sup>2</sup> and P. Venkatakrishnan<sup>1</sup>

<sup>1</sup> Udaipur Solar Observatory, Physical Research Laboratory, Dewali, Badi Road, Udaipur 313 004, India  
*bayanna@prl.res.in*

<sup>2</sup> Leibniz-Institut für Astrophysik Potsdam (AIP), An der Sternwarte 16, 14482, Potsdam, Germany

**Abstract** We present properties of intensity oscillations of a sunspot in the photosphere and chromosphere using G band and Ca II H filtergrams from *Hinode*. Intensity power maps as function of magnetic field strength and frequency reveal reduction of power in G band with increase in photospheric magnetic field strength at all frequencies. In Ca II H, however, stronger fields exhibit more power at high frequencies particularly in the 4.5 mHz–8.0 mHz band. Power distribution in different locations of the active region show that the oscillations in Ca II H exhibit more power in comparison to that of G band. We also relate the power in intensity oscillations with different components of the photospheric vector magnetic field using near simultaneous spectro-polarimetric observations of the sunspot from the *Hinode* spectropolarimeter. The photospheric umbral power is strongly anti-correlated with the magnetic field strength and its the line-of-sight component while there is a good correlation with the transverse component. A reversal of this trend is observed in the chromosphere with the exception at low frequencies ( $\nu \leq 1.5$  mHz). The power in sunspot penumbrae is anti-correlated with the magnetic field parameters at all frequencies ( $1.0 \leq \nu \leq 8.0$  mHz) in both the photosphere and chromosphere, except that the chromospheric power shows a strong correlation in the frequency range 3–3.5 mHz.

**Key words:** Sun: photosphere – Sun: chromosphere – Sun: Oscillations – Sun: Magnetic fields – Sun: *Hinode*

## 1 INTRODUCTION

Over the years, a wide range of oscillatory phenomena have been observed in various regions of the Sun. Oscillations in the solar atmosphere have been studied since 1960s (Leighton, Noyes & Simon 1962). These studies have improved our understanding of the internal structure of the Sun as well as the dynamic structure of sunspots. Intensity, velocity and magnetic field observations of the Sun in various spectral lines have been

The studies related to the photosphere emphasize on understanding the internal structure of the Sun through acoustic waves, while the studies with the chromospheric lines focus on understanding the propagation of waves to the higher atmosphere, their interaction with the magnetic fields there, and consequently understanding the problem of coronal heating.

The important findings of these studies in magnetic media are: (i) the presence of the photospheric five minute oscillations, and its absorption in the regions of strong photospheric magnetic fields (Braun et al. 1987, 1988, 1992, 1994; Bogdan et al. 1993; Hindman & Brown 1998; Kumar et al. 2000; Jain & Haber 2002; Venkatakrishnan et al. 2002), (ii) enhanced oscillations in chromospheric umbra in the three minute band (Bhatnagar & Tanaka 1972; Lites 1986; Kentischer & Mattig 1995; Nagashima et al. 2007), and (iii) running penumbral waves (Zirin & Stein 1972; Giovanelli 1972, 1974; Maltby 1975; Christopoulou et al. 1999, 2000, 2001; Bloomfield et al. 2007). Some of the review articles (Bogdan 2000, Solanki 2003, Bogdan & Judge 2006) explain the work done on the nature of sunspot oscillations and related problems. In this context, simultaneous time-series observations in various spectral lines that sample the sunspot atmosphere at different heights using high resolution instruments such as the Solar Optical Telescope (SOT) (Tsuneta et al. 2008) on board *Hinode* (Kosugi et al. 2007) and the Helioseismic and Magnetic Imager (Schou et al. 2012) on board *Solar Dynamics Observatory* (SDO; Pesnell et al. 2011) can be useful in studying these oscillatory processes and their contribution to the dynamics in the solar atmosphere.

The high-resolution and multi-wavelength capability of *Hinode* provide several important opportunities to local helioseismologists. These allow to understand and confirm many physical processes in the sub-surface layers of the Sun and also in its atmosphere (Sekii 2009; Kosovichev 2012), some of which are as follows. Nagashima et al. (2007) studied intensity oscillations in a sunspot and showed that G band power is suppressed in sunspot umbra, while Ca II H observations revealed high-frequency oscillations with a peak at 6 mHz. Kosovichev & Sekii (2007) studied the flare-induced high-frequency chromospheric oscillations in a sunspot. Sekii et al. (2007) confirmed that the supergranulation is a shallow phenomenon. Similarly, Mitra-Kravez et al. (2008) examined the phase difference between oscillations of the photosphere and chromosphere. Zhao et al. (2010) obtained travel-time measurements for short distances without phase-speed filtering and confirmed the sound-speed results, which were obtained using data from Michelson Doppler Imager (MDI) (Scherrer et al. 1995) on board the *Solar and Heliospheric Observatory* (*SoHO*; Domingo et al. 1995) with the phase-speed filtering.

We study intensity fluctuations in different regions of an active region and the correlation between the different parameters of the photospheric magnetic fields and the intensity oscillatory power at different heights in the solar atmosphere in different frequency bands using *Hinode*/SOT data. Earlier investigations carried out by Mathew (2008) using Dopplergrams from *SoHO*/MDI and potential field computations from *SoHO*/MDI line-of-sight magnetograms revealed that the umbra-penumbra boundary showed enhanced absorption of power, where the transverse potential field was strongest. Gosain et al. (2010) confirmed the aforementioned result by relating the power obtained from *SoHO*/MDI Dopplergrams with a vector magnetogram obtained from *Hinode*. Using high-resolution observations of G band and Ca II H obtained from *Hinode*, Nagashima et al. (2007) studied the power in spatial scales corresponding to umbral flashes and

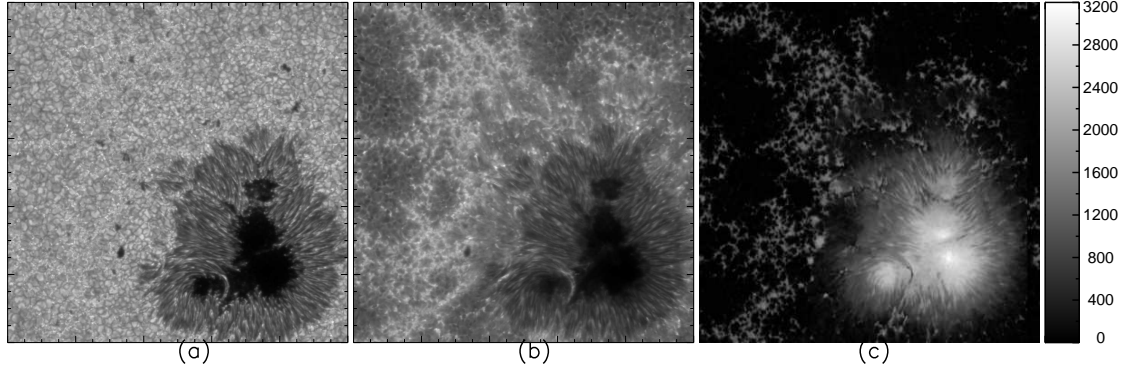


**Fig. 1** Intensity filtergrams of the active region NOAA 10953 in: (a) G band and (b) Ca II H line with a field-of-view of  $112 \text{ arc-sec}^2$ . The magnetic field strength map is shown in (c).

all frequencies. To that end, we employ high temporal and spatial resolution observations from *Hinode* to study the nature of sunspot oscillations and its relation to the photospheric magnetic field parameters.

## 2 THE OBSERVATIONAL DATA

We have used a 3 hr 30 min sequence of G band and Ca II H filtergrams of the active region NOAA 10953 recorded by the Broad-band Filter Imager (BFI) of the *Hinode*/SOT to study the intensity oscillations in the active region. The filtergrams were acquired on 2007 May 1 during 14:31-17:57 UT and have a spatial sampling of  $0''.11 \text{ pixel}^{-1}$  and a cadence of one minute. The active region was located at S10W05 on the solar disk. The field-of-view (FOV) of the filtergrams is  $112 \text{ arc-sec}^2$ . G band filtergrams were acquired nearly 3 s later to Ca II H filtergrams. In-addition to the broad band images, near simultaneous spectro-polarimetric observations of the active region from SOT/SP (Ichimoto et al. 2008) have been used in our analysis. SOT/SP records the four Stokes spectra of the Fe line pair at 630 nm with a spectral sampling of  $21.5 \text{ m\AA}$  and an exposure time of 4.8 s at each slit position. We have used level-2 maps comprising magnetic field strength, inclination, and azimuth which were obtained by inverting the observed Stokes profiles employing the MERLIN<sup>1</sup> code. The active region was scanned in the fast mode with a step width of  $0''.29$  and a sampling of  $0''.32$  along the slit. These maps were interpolated to a spatial scale of  $0''.32 \text{ pixel}^{-1}$  in both the directions. Consequently, the images obtained with BFI were also re-scaled to  $0''.32 \text{ pixel}^{-1}$  resolution to match that of the SOT/SP maps.

## 3 ANALYSIS AND RESULTS

The images were corrected for flat-fielding, dark current and bad pixels using standard Solarsoft routines. Although, the correlation tracker is employed to take care of global motion of the region of interest, we performed a rigid alignment of the sunspot as a function of time. This was done using a FFT based 2D cross-correlation routine, updating the reference frame at every  $10^{\text{th}}$  frame to account for the evolution of the sunspot. Figure 1 shows the snapshot of the active region in G band and Ca II H along the map of magnetic field strength. Figure 2 shows time averaged G band and Ca II H images deduced over the period

14:31-17:57 UT on 2007 May 1. The average images were normalized with their exposure times to obtain the counts in same scale in both the images.

A two point backward difference filter (García & Ballot, 2008) was applied to obtain the first difference of the time series and the filtered data were normalized by the mean intensity in the two running frames as shown in the equation (1). First difference enhances the oscillatory signals above the background variations and the normalization by the mean intensity causes a smooth transition between the umbra and the penumbra (Nagashima et al. 2007).

$$\hat{I}_k = 2 (I_k - I_{k-1}) / (I_k + I_{k-1}) \quad (1)$$

Where,  $\hat{I}_k$  and  $I_k$  are normalized intensity and intensity of the  $k^{th}$  image of the sequence, respectively.

Further, we computed the Power Spectral Density (PSD) from the mean normalized differential intensity fluctuations at each pixel and generated 3D power maps with frequency along the z-direction. PSD in each pixel is corrected for  $\omega^2$  to remove the effect of the time-derivative (Nagashima et al. 2007). The variation of intensity oscillatory power in different regions of the active region in G band and Ca II H observations are studied in the following sections.

### 3.1 Power distribution in different regions of the active region and quiet Sun

In order to investigate the power distribution in different regions of the active region, the FOV was divided into the following regions: umbra, umbra-penumbra boundary (UPB), penumbra, plage, and quiet Sun. The iso-intensity contours overlaid on the time averaged G-band and Ca II H images in Figure 2 were determined from the peaks in the intensity distribution. The contours enclosing the umbra, UPB, and penumbra were obtained from the time averaged G-band image while the same for the plage region was determined from the time averaged Ca image; the bright regions outside the sunspot are considered as plage while the regions that

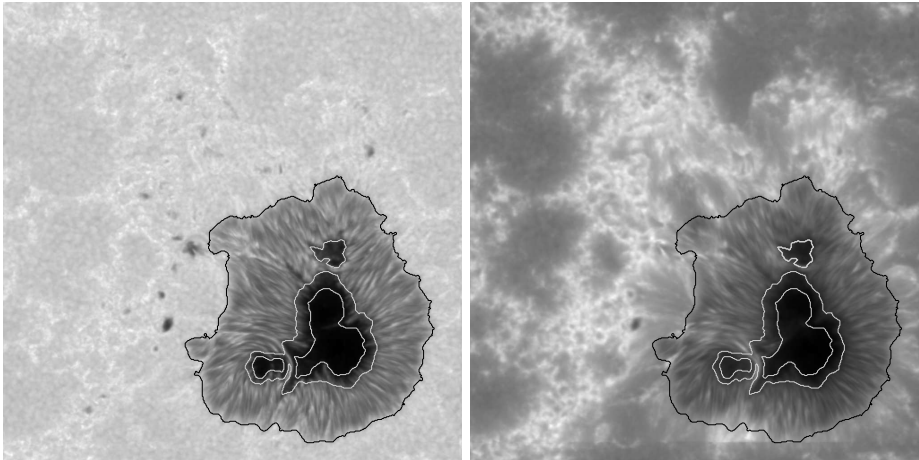


**Fig. 2** Average intensity maps of the active region in G band (left) and Ca II H line (right). The contours correspond to umbra, umbra-penumbra boundary, penumbra and quiet Sun. The bright regions outside the sunspot are considered as plage while the regions that are neither bright in G band and Ca II H are assumed to be quiet Sun.

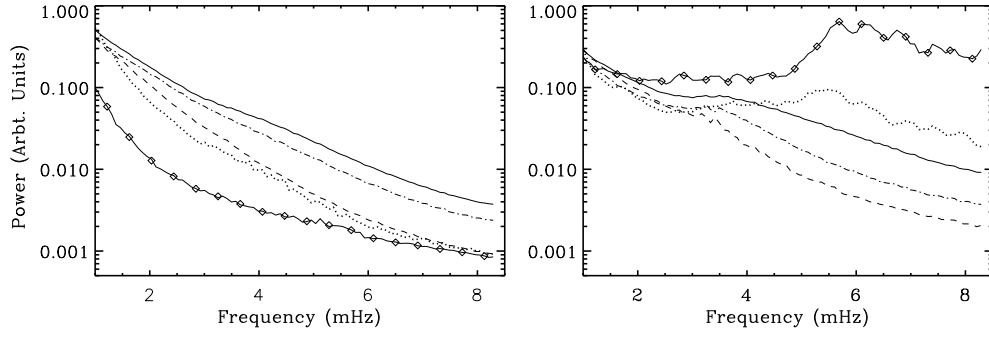


**Fig.3** Power distribution of G band intensity (left) and Ca II H intensity (right) in different regions of the FOV. Power in umbra (solid line with diamond symbols), umbra-penumbra boundary (dotted line), penumbra (dashed line), plage (dot-dashed) and quiet Sun (solid line) are shown here.

are neither bright in G band and Ca II H are assumed to be quiet Sun. The fraction of pixels corresponding to umbra, UPB, and penumbra are 0.022, 0.030, 0.22, respectively. Plage region and quiet region contain 0.626 and 0.091 fraction of pixels, respectively. The average power in each of these regions as a function of frequency is shown in Figures 3 and 4. Figure 3 allows us to compare the power in the different regions described above, separately in G band and Ca II H. On the other hand, Figure 4 shows a comparison between the powers in G band and Ca II H in each of the regions.

It is observed that intensity oscillatory power in G band decreases from the quiet Sun to umbra (i.e., in the order quiet Sun, plage, penumbra, UPB, and umbra) at all frequencies. On the other hand, power in Ca II H shows such a trend from quiet Sun to penumbra only, with the exception of slight enhancement of power in 3-4 mHz frequency range (c.f., Figure 3). It is also observed that overall power is lower in G band as compared to Ca II H with a cross-over seen at 3 mHz which shifts to 0 mHz as we move from the quiet Sun to the umbra of the sunspot (c.f. Figure 4). Thus, Ca II H oscillations are seen to be richer in high-frequency power in the magnetized environment, which is in good agreement with the results of

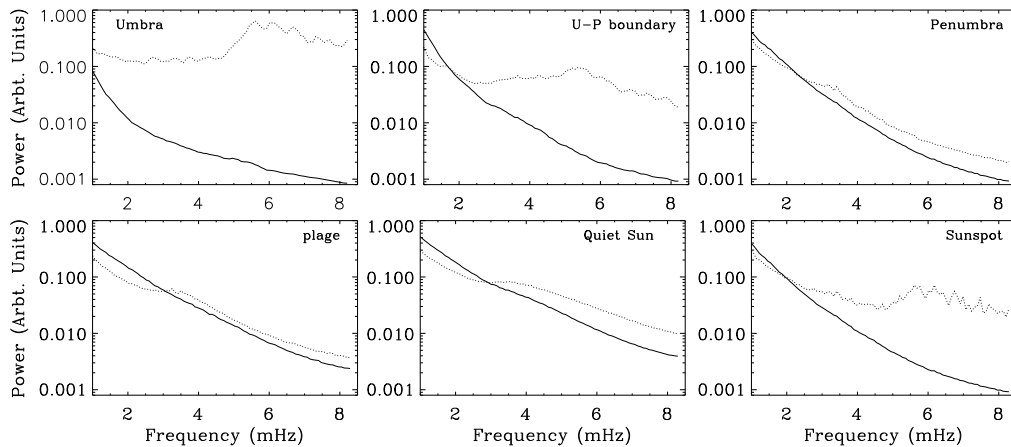


**Fig.4** Power distribution of G band intensity (solid line) and Ca II H intensity (dotted line) in the regions: umbra (top-left), umbra-penumbra boundary (top-middle), penumbra (top-right), plage (bottom-left), quiet Sun (bottom-middle) and sunspot (bottom-right).

Nagashima et al. (2007). We also observe the presence of 5-minute oscillations in quiet Sun, plage and penumbral regions.

### 3.2 Intensity power maps as function of magnetic field strength and frequency

In order to examine the relation between oscillatory power in G band and Ca II H with respect to the photospheric magnetic field strength ( $B$ ) and frequency, we constructed power maps as function of magnetic field strength and frequency as indicated in Figure 5. These maps were derived by averaging the power in all pixels having similar magnetic field strengths over a 30 G interval at each frequency ranging from 0.1 to 8.3 mHz. We observe the following from these power maps.

1. In general, Ca II H shows larger power in comparison to that of G band for any magnetic field strength and frequencies above 1 mHz.
2. Power in G band decreases with increase in magnetic field strength at all frequencies.
3. Ca II H shows larger power in stronger magnetic fields ( $|B| > 2200$  G) at all frequencies and less power in the intermediate field regime ( $100 \text{ G} < |B| < 2000$  G) at frequencies above 5 mHz. Weaker fields ( $|B| < 100$  G) show larger power in the frequency range 0-6 mHz in comparison to the same in the intermediate field strength regime.
4. Power map of Ca II H is more structured than that of G band. It shows the signature of 5-minute oscillations for the magnetic field strengths between 1200-2000 G. These fields are mostly located in the penumbral region where the inclination is in the range of 90-130 degrees. In the higher magnetic field regions (mostly, umbra) it also shows oscillatory behavior.

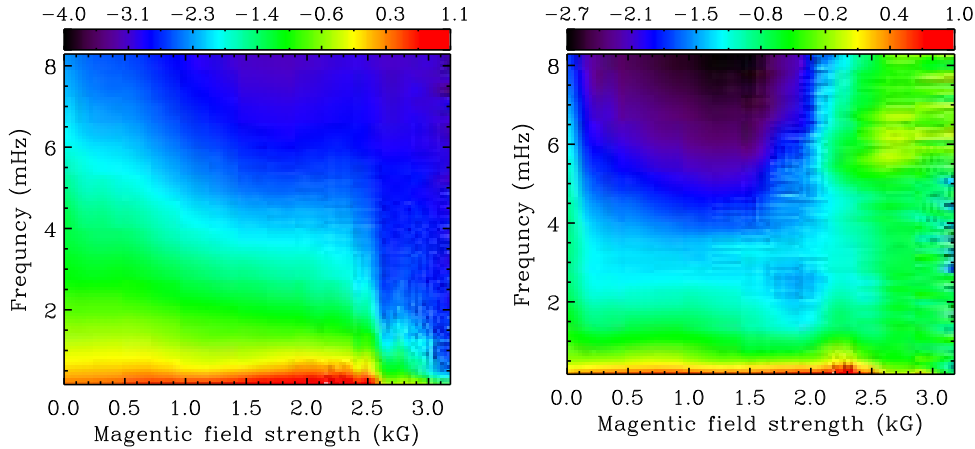


**Fig. 5** Power maps from the intensity variations in the active region NOAA 10953 in G band (left) and Ca II H (right) as function of magnetic field strength and frequency. The maps are shown in logarithmic scale as indicated by the color bar.

### 3.3 Relation between magnetic field parameters and oscillatory power in the sunspot

The radial variation of the observed magnetic field parameters is studied using the enclosed curves shown in Figure 6. The umbra-penumbral boundary and penumbra-quiet Sun boundary obtained from the time-



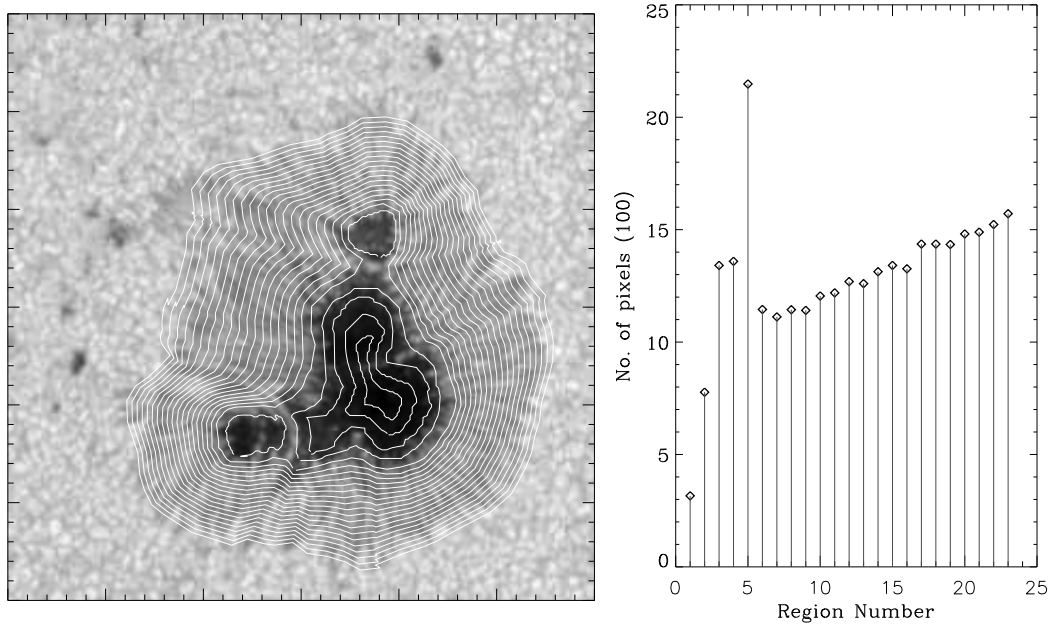


**Fig. 6** Left: Enclosed curves overlaid on the intensity filtergram of the active region to study the radial and azimuthal variation of the magnetic field parameters and oscillations in various regions of the sunspot. Right: The number of pixels enclosed by each annular-like region are shown in the plot. The regions are numbered from center of umbra to sunspot boundary.

azimuthal direction which yielded the curves shown in Figure 6. The curves inside the umbra were hand drawn, which are separated by  $\approx 1''$ . The other curves between umbra-penumbra boundary and penumbra are spaced apart by  $0''.6$ . The regions 1-3 and 8-20 correspond to umbra and penumbra, respectively, while the regions 4-7 represent the umbra-penumbra boundary. The number of pixels enclosed by each region is illustrated in Figure 6.

The azimuthally averaged radial profiles of various magnetic field parameters are shown in Figure 7. It is observed that magnetic field strength ( $B$ ), inclination ( $\gamma$ ), and line-of-sight ( $B_l$ ) components of magnetic field show smooth variation with the radial distance. Transverse component of magnetic field ( $B_t$ ) increases from center of the umbra to the inner-mid penumbra and, thereafter, this trend reverses. The vertical bars correspond to  $\pm 1\sigma$  errors in the estimated values. In general, the power in umbra-penumbra boundary (regions 4-7) and sunspot-quiet Sun boundary (regions 21-23) shows relatively larger spread in G band. Whereas in Ca II H, the power in umbra and umbra-penumbra boundary shows larger spread.

The radial variation of power in Ca II H is dominant in the umbra in comparison to the other regions of the sunspot in the frequency regimes 2-5 mHz and 5-8 mHz. On the other hand, in 0-2 mHz band umbra-penumbra boundary shows enhancement of power both in Ca II H and G band. Umbra-penumbra boundary in Ca II H shows reduction of power in 2-5 mHz and 5-8 mHz bands, while it shows enhancement of power in G band for the above frequency ranges. This reduction/enhancement of power at umbra-penumbra boundary occurs around the peak value of the transverse magnetic field. The inclination of magnetic field

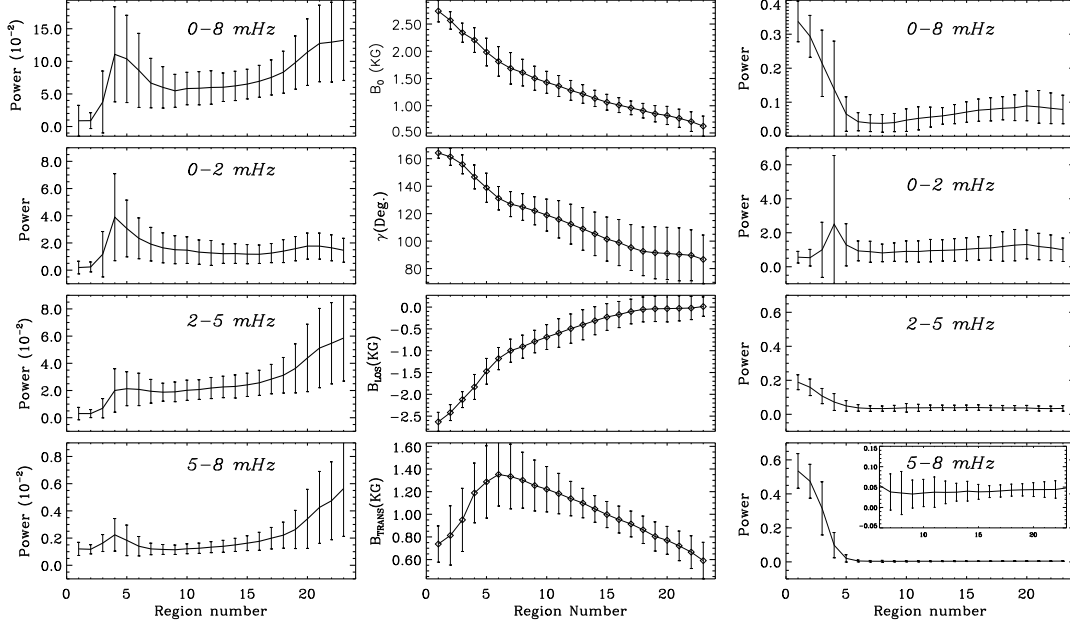


**Fig.7** Radial variation of power in G band and Ca II H are shown in left and right panels, respectively. Corresponding variation of magnetic field parameters ( $B$ ,  $\gamma$ ,  $B_l$  and  $B_t$ ) are shown in the middle panels. The power is averaged over frequency regimes: 0-8 mHz, 0-2 mHz, 2-5 mHz and 5-8 mHz. The vertical bars show  $\pm 1\sigma$  errors in the estimated values. The regions 1-3, 4-7 and 8-20 correspond to umbra, umbra-penumbra boundary and penumbra, respectively. The regions 21-23 correspond to sunspot-quiet Sun boundary.

obtained by MDI/*SoHO* showed enhanced  $p$ -mode absorption near umbra-penumbra boundary, where the inclination angle is nearly  $135^\circ$  (Mathew 2008; Gosain et al. 2010).

In order to understand the relation between magnetic field parameters and intensity oscillatory power of the sunspot, we estimated the correlation-coefficients between radial variation of power and the magnetic field parameters averaged over each region. Here, it is observed that none of the magnetic field parameters ( $B$ ,  $B_l$ , and  $B_t$ ) show any correlation with the power in the sunspot. A Similar analysis by Gosain et al. (2010) did not reveal any strong association of the magnetic field parameters with Doppler power in a sunspot. However, when we derive the correlation-coefficients separately for the umbra and penumbra, we find distinct relations between the magnetic field parameters and the PSD which are shown in Figure 8. When we consider sunspot as a whole, the distinct behaviors in the umbra and penumbra gets mixed-up and thus there is no correlation seen in our analysis.

Intensity oscillatory power in Ca II H penumbra shows anti-correlation with  $B$ ,  $|B_l|$  and  $B_t$  at all the frequencies except in the frequency range of 3.0-3.5 mHz, i.e. in the 5-minute regime. G band intensity power in penumbra also shows anti-correlation with magnetic field parameters. Similarly, the umbral power in Ca II H shows correlation with  $B$ , and  $|B_l|$  above 1.5 mHz and opposite relation with  $B_t$ . Whereas, G band umbral power shows completely opposite trend; i.e. it does show anti-correlation with  $B$  and  $|B_l|$ ,



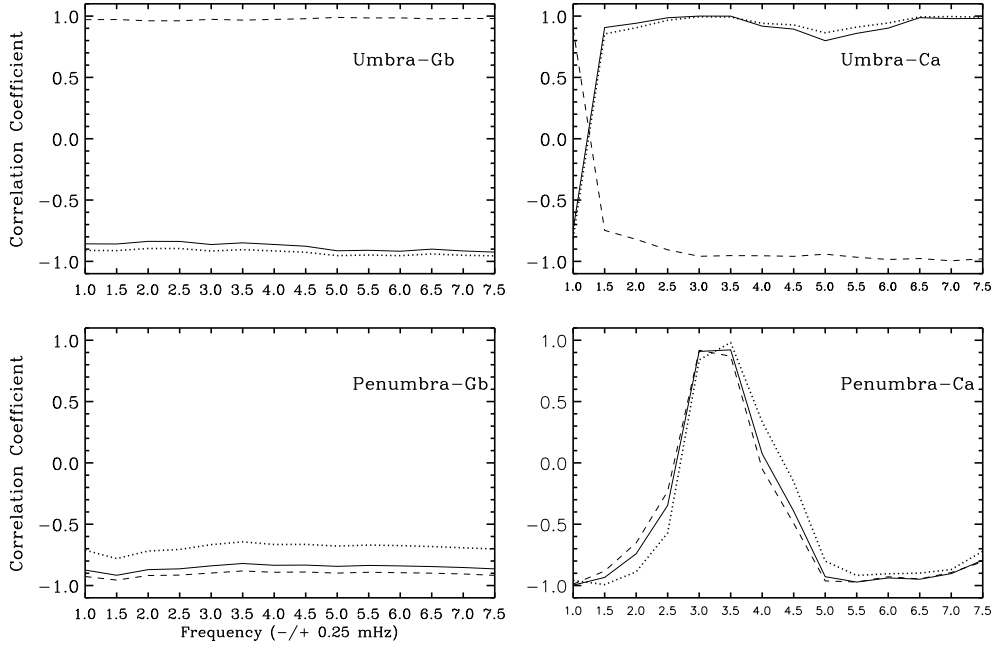


**Fig. 8** Plots show correlation between the photospheric magnetic field parameters and intensity oscillatory power of umbra (top-panels) and penumbra (bottom panels) in G band (left panels) and Ca II H (right panels) in different frequency bands. Correlation between  $B$  vs. power (solid line),  $B_t$  vs. power (dashed line), and  $B_l$  vs. power (dotted) are shown here.

#### 4 SUMMARY AND DISCUSSION

We have analyzed high-resolution G band and Ca II H line filtergrams of the active region NOAA 10953 obtained by *Hinode*/SOT along with near simultaneous spectro-polarimetric observations of this active region from *Hinode* SOT/SP to study the relation between various magnetic parameters and the intensity oscillatory power in the photosphere and chromosphere. Our chief findings are as follows:

1. Photospheric power maps derived from G band time series reveal more power in the quiet Sun (weaker fields) in comparison to the sunspot. This is in agreement with the previous reports that stronger magnetic fields absorb more power in the 5-minute band (Braun et al. 1992; Hindman & Brown 1998; Kumar et al. 2000; Venkatakrishnan et al. 2002, and references therein). We, however, do not observe a reversal of this trend at higher frequencies in magnetic concentrations as shown by Venkatakrishnan et al. (2002) in oscillatory power derived from photospheric Dopplergrams. Our analysis showing the absence of photospheric power at high frequencies in strong magnetic field regions is consistent with the results of Jain & Haber (2002) who reported that only power spectra derived from Dopplergrams exhibit the above trend and not from intensity filtergrams. We emphasize here that the well known 5-minute oscillations are not dominantly seen in G band power maps, whereas the 5-minute oscillations have been distinctly observed by Jain & Haber (2002) in the continuum intensity power of the data obtained from *SoHO*/MDI.

To confirm this, we have analyzed Dopplergrams and continuum intensity images obtained by the

on 2013 April 11. We estimated the PSD of the quiet Sun near the disk center for both the data sets. The Dopplergrams exhibit dominant power in 5-minute regime and similar nature of power is also observed in the continuum intensity images. However, the power in intensity is weaker in comparison to the Doppler power in the 5-minute regime. These results obtained with *SDO/HMI* is in agreement with the work done by Jain & Haber (2002) using the data obtained from *SoHO/MDI*. We conjecture that the reason behind the observed lower power of 5-minute oscillations in G band data relative to that in continuum intensity power from *SoHO/MDI* and *SDO/HMI* could be due to difference in their formation heights in the solar atmosphere.

2. It is well known that in the chromosphere, the umbra shows an enhancement in power at frequencies above 5 mHz (Bhatnagar & Tanaka 1972; Braun et al. 1992; Brown et al. 1992; Kentischer & Mattig 1995; Lites 1986). We also observe such a behavior in our analysis of Ca II H power (c.f., Figure 3 and 5). The umbral 3-minute chromospheric oscillations are suggested to emanate directly from the photosphere through linear wave propagation (Centeno et al. 2006). Spectropolarimetric investigations by Centeno et al. (2006) using simultaneous observations taken in photosphere and chromosphere have provided observational evidence for the upward propagation of slow magneto-acoustic waves from the photosphere to the chromosphere inside the umbra of a sunspot. The phase spectra derived by Centeno et al. (2006) yield a value of the atmospheric cut-off frequency around 4 mHz and shows evidence for the upward propagation of higher frequency oscillations. Similarly, the presence of 5-minute oscillations in the chromospheric quiet Sun, and penumbral regions is attributed to the inclined magnetic field lines along which the photospheric 5-minute oscillations propagate to the higher atmosphere (Jefferies et al. 2006; McIntosh & Jefferies 2006).
3. We have used near simultaneous *Hinode* SOT/SP observations of an active region, close to disk-center, to study the relationship between the magnetic-field parameters and the intensity oscillatory power in G band and Ca II H. The azimuthally averaged radial profiles of field strength and inclination show a smooth decrease from the centre of the umbra to the periphery of the sunspot (c.f., Figure 7). However, the power does not exhibit a similar behavior. Umbra in Ca II H and G band shows reduction of power in 0-2 mHz band. While this behavior is illustrated at all other frequencies in G band, the same shows enhancement in 5-8 mHz band in Ca II H. The umbra-penumbra boundary shows enhancement of G band power at all frequencies, where the transverse magnetic field is the highest.
4. The correlation analysis to the umbra and penumbra, separately, shows correlation between power and magnetic field parameters. In order to examine the influence of magnetic field on oscillatory power, we determined the correlation as a function of frequency bins. We observe that the photospheric magnetic parameters (except the transverse component) are correlated with umbral power in Ca II H and anti-correlated with umbral power in G band at all frequencies, while the transverse magnetic field exhibits the opposite result. However, the analysis that includes only the penumbra shows that G band power in the penumbra is anti-correlated with magnetic field parameters at all frequencies. Ca II H power in penumbra shows strong correlation with photospheric magnetic field in the frequency band 3.0-3.5 mHz, while at every other frequencies they are anti-correlated.

The observed correlation between chromospheric penumbral power and photospheric magnetic fields in the 5-minute band could be the result of the magnetic inclination becoming large enough to allow photospheric 5-minute power to tunnel through higher acoustic cut-off frequency as demonstrated by Bloomfield et al. (2007) using simultaneous spectro-polarimetric observations of photosphere and chromosphere. As the umbral 3-minute chromospheric oscillations are inferred as field-aligned propagating slow magneto-acoustic waves (Centeno et al. 2006), the observed correlation between photospheric magnetic fields and the chromospheric umbral power could also be due to the transportation of the photospheric power to the chromosphere through the magnetic field lines.

**Acknowledgements** *Hinode* is a Japanese mission developed and launched by ISAS/JAXA, collaborating with NAOJ as a domestic partner, NASA and STFC (UK) as international partners. Scientific operation of the *Hinode* mission is conducted by the *Hinode* science team organized at ISAS/JAXA. This team mainly consists of scientists from institutes in the partner countries. Support for the post-launch operation is provided by JAXA and NAOJ (Japan), STFC (U.K.), NASA (U.S.A.), ESA, and NSC (Norway). We also thank Community Spectro-polarimetric Analysis Center team at High-Altitude Observatory for providing the vector magnetogram (level2) data. Thanks to B. Ravindra for his valuable suggestions related to this work. Rohan E. Louis is grateful for the financial assistance from the German Science Foundation (DFG) under grant DE 787/3-1. We thank the anonymous referee for constructive comments and suggestion that improved the presentation of the manuscript.

## References

- Bhatnagar, A. and Tanaka, K., 1972, *Sol. Phys.*, 24, 87
- Bogdan, T. J., Brown, T. M., Lites, B. W. and Thomas, J. H., 1993, *ApJ*, 406, 723
- Bogdan, T. J., 2000, *Sol. Phys.*, 192, 373
- Bogdan, T. J. and Judge, P. G., 2006, *Royal Society of London Philosophical Transactions Series A*, 364, 313
- Bloomfield, D. S., Lagg, A. and Solanki, S. K., 2007, *ApJ*, 671, 1005
- Braun, D. C., Duvall, Jr., T. L. and Labonte, B. J., 1987, *ApJ*, 319, L27
- Braun, D. C., Duvall, Jr., T. L. and Labonte, B. J., 1988, *ApJ*, 335, 1015B
- Braun, D. C., Duvall, Jr., T. L. and Labonte, B. J., 1992, *ApJ*, 391, L113
- Braun, D. C., Labonte, B. J. and Duvall, Jr., T. L. et al., 1993, *Astron. Soc. Pac. Conf. Series*, 42, 77
- Brown, T. M., Bogdan, T. J., Lites, B. W., Thomas, J. H., 1992, *ApJ*, 394, L65
- Centeno, R. and Collados, M. and Trujillo Bueno, J., 2006, *ApJ*, 640, 1153
- Christopoulou, E. B., Georgakilas, A. A. and Koutchmy, S. 1999, *Astron. Soc. Pac. Conf. Series*, 184, 103
- Christopoulou, E. B., Georgakilas, A. A. and Koutchmy, S. 2000, *A&A*, 354, 305
- Christopoulou, E. B., Georgakilas, A. A. and Koutchmy, S. 2001, *A&A*, 375, 617
- Domingo, V., Fleck, B., & Poland, A. I., 1995, *Sol. Phys.*, 162, 1
- García, R. A. and Ballot, J., 2008, *A&A*, 477, 611
- Giovanelli, R. G., 1972, *Sol. Phys.*, 27, 71
- Giovanelli, R. G., 1974, *IAU Symposium*, 56, 137
- Gosain, S., Mathew, S. K. and Venkatakrishnan, P., 2011, *Sol. Phys.*, 268, 335
- Hindman, B. W. and Brown, T. M., 1998, *ApJ*, 504, 1029
- Ichimoto, K., Lites, B. and Elmore, et al., 2008, *Sol. Phys.*, 249, 233
- Jain, R. and Haber, D., 2002, *A&A*, 387, 1092
- Jefferies, S. M. and McIntosh, S. W. and Armstrong et al., 2006, *ApJ*, 648, L151
- Kentischer, T. J. and Mattig, W., 1995, *A&A*, 300, 539
- Kosovichev, A. G. and Sekii, T., 2007, *ApJ*, 670, L147

- Kosovichev, A. G., 2012, *Sol. Phys.*, 279, 323
- Kosugi, T., Matsuzaki, K., and Sakao, et al., 2007, *Sol. Phys.*, 243, 3
- Kumar, B., Jain, R. and Tripathy, et al., 2000, *Sol. Phys.*, 191, 293
- Leighton, R. B., Noyes, R. W. and Simon, G. W., 1962, *ApJ*, 135, 474
- Lites, B. W., 1986, *ApJ*, 301, 1005
- Nagashima, K., Sekii, T. and Kosovichev, A. G., et al., 2007, *PASJ*, 59, 631
- Maltby, P., 1975, *Nature*, 257, 468
- Mathew, S. K., 2008, *Sol. Phys.*, 251, 515
- McIntosh, S. W. and Jefferies, S. M., 2006, *ApJ*, 647, L77
- Mitra-Kraev, U., Kosovichev, A. G. and Sekii, T., *A&A*, 2008, 281, L1
- Pesnell, W. D., Thompson, B. T., and Chamberlin, P. C., 2011, *Sol. Phys.*, 275, 3
- Schou, J., Scherrer, P. H. and Bush, R. I. et al., 2012, *Sol. Phys.*, 275, 229
- Scherrer, P. H., Bogart, R. S. and Bush, et al., 1995, *Sol. Phys.*, 162, 129
- Sekii, T., Kosovichev, A. G. and Zhao, J. et al., 2007, *PASJ*, 59, 637
- Sekii, T., 2009, *Astron. Soc. Pac. Conf. Series*, 415, 405
- Solanki, S. K., 2003, *A&A Rev.*, 11, 153
- Staude, J., 1999, *Astron. Soc. Pac. Conf. Series*, 184, 113
- Staude, J., 2002, *Astronomische Nachrichten*, 323, 317
- Tsuneta, S., Ichimoto, K. and Katsukawa, Y. et al., 2008, *Sol. Phys.*, 249, 167
- Venkatakrishnan, P., Brajesh Kumar, and Tripathy, S. C., 2002, *Sol. Phys.*, 387, 642
- Zhao, J., Kosovichev, A. G. and Sekii, T., 2010, *ApJ*, 708, 304
- Zirin, H. and Stein, A., 1972, *ApJ*, 178, L85
-